Structural Transitions in Geometrically Frustrated Smectics

Jingmin Xia,[1] Scott MacLachlan,[2] Timothy J. Atherton,[3] and Patrick E. Farrell[1]

[1]*Mathematical Institute, University of Oxford, Oxford, UK*
[2]*Department of Mathematics and Statistics, Memorial University of Newfoundland, St. John's, NL, Canada*
[3]*Department of Physics and Astronomy, Tufts University, Medford, MA 02155, USA*

A phenomenological free energy model is proposed to describe the behavior of smectic liquid crystals, an intermediate phase that exhibits orientational order and layering at the molecular scale. Advantageous properties render the functional amenable to numerical simulation. The model is applied to a number of scenarios involving geometric frustration, leading to emergent structures such as focal conic domains and oily streaks and enabling detailed elucidation of the very rich energy landscapes that arise in these problems.

I. INTRODUCTION

Smectic liquid crystals are complex fluids that exhibit orientational order and a layered structure over macroscopic distances [1]. Since the layers are nearly incompressible, an immediate consequence is that the material prefers to locally adopt one of six families of surfaces (in three dimensions) compatible with constant layer spacing [2–5]. External constraints may force deformations of the smectic that are incompatible with the layer constraint, leading to geometric frustrations and the spontaneous assembly of a wide variety of textures with characteristic defect structures of the smectic phase [4, 6]. Driven by advances in surface control, there has been considerable renewed interest in exploiting the ability of smectics to repeatably self-assemble over device length-scales by using surface patterning [7, 8], topographical features such as grooves [9–12] or posts [13, 14], confinement in droplets [15–17] or curved surfaces more generally [18], to produce emergent patterns [19, 20] that are optically active as lenses, gratings [21], photonic crystals [20] or lithographic templates [22]. Moreover, defect structures in the texture act to efficiently trap dispersed micro- or nanoparticles, making smectics useful for hierarchical [23–25] or synergistic [26] assembly processes that are potentially useful for metamaterial, sensor or solar cell production. Since many of the remarkable properties of smectics arise because of the geometric and topological consequences of layering, they form a paradigmatic model system to understand geometric frustration in other lamellar phases such as block copolymers [27, 28], membranes and vesicles [29, 30].

The very complicated structures that emerge in frustrated smectics have, however, proven to be very challenging to model mathematically. While many of the observed textures have been understood through elegant geometric approaches [3, 4, 13, 18–20, 26, 31–35], or by perturbing from the nematic phase [36–38], to date there have been few successful efforts to use numerical methods to predict the structures adopted by smectics in general configurations. Such methods could be of great benefit to structure prediction where the defects cannot be observed optically, for example in thin films [39–43]. Furthermore, scenarios where partial smectic order exists, such as during the transition from the nematic to the smectic phase, may exhibit very complicated pre-transitional structures [37, 38, 44, 45] and few studies have addressed the connection between pattern formation and the peculiar critical behavior of liquid crystals at the nematic-smectic transition [46]. Dynamical phenomena, such as time-varying layer spacing [47], interactions between embedded particles [31] and the evolution of smectic films and bubbles [48–50] also present difficult problems that appear to require numerical modelling.

One major obstacle to successful modelling of smectics is the complicated nature of the smectic order. In the original theory of de Gennes [1], the smectic phase is characterized by a complex order parameter $\psi(\mathbf{r}) = |\psi(\mathbf{r})|e^{i\phi(\mathbf{r})}$ that contains both the amplitude and phase of the density modulations. It is a remarkably successful approach, providing a theory of the nematic-smectic-A transition analogous to the Ginzburg–Landau theory of superconductivity. Nonetheless, it presents certain challenges, as reviewed in Pevnyi et al. [51]. The first issue is due to the topology of the complex order parameter ψ itself: $\text{Im}(\psi)$ does not contain physical information. Second, this model is formed on a *coarse-grained* basis, i.e., this energy does not represent the local free energy density on the length scale of the smectic layers themselves. To amend these issues, Pevnyi et al. propose a theory formulated in terms of a real-valued variation $\delta\rho(\mathbf{r})$ from the average density and a director field $\mathbf{n}(\mathbf{r})$, the local axis of average molecular alignment. Using a real-valued density variation avoids many of the problems of alternative approaches such as using double-valued complex order parameters [51]. Nonetheless, this theory as presented is not able to reproduce half-charge defects, due to the presence of director discontinuities in these defects [52], which cannot be characterized by a continuous vector field. For example, around a $\pm 1/2$ defect where $\mathbf{n}$ rotates by $\pm\pi$ degrees, a discontinuity line where $\mathbf{n}$ reverses sign must exist. In fact, since $\mathbf{n}$ enters the model only through the tensor $\mathbf{n} \otimes \mathbf{n} = \mathbf{n}_i\mathbf{n}_j$, Pevnyi et al. solve for this tensor instead in their implementation. This allows

them to represent half-charge defects [52], but numerically enforcing the rank-one constraint in minimization is difficult [53].

In this work, we formulate a theory of smectics suitable for finite element simulation and apply it to several partially understood problems involving the configuration of smectics between antagonistic boundary conditions, i.e., those that favor opposing orientations incompatible with the layer constraint. We quantitatively study the transition from uniform layering to the formation of defects [54], examine the role of pretilt on the configuration of focal conic domains [44] and predict the structure of oily streaks that occur in very thin smectic films [21, 41, 43].

II. OUR MODEL

We begin with Pevnyi et al.'s proposed energy [51],

$$F(\delta\rho, \mathbf{n}) = \int_\Omega \left[\frac{a}{2} (\delta\rho)^2 + \frac{b}{3} (\delta\rho)^3 + \frac{c}{4} (\delta\rho)^4 \right.$$
$$\left. + B \left| \mathcal{D}^2 \delta\rho + q^2 \mathbf{n} \otimes \mathbf{n} \delta\rho \right|^2 + \frac{K}{2} |\nabla \mathbf{n}|^2 \right], \quad (1)$$

which is to be extremized to obtain stationary solutions $\delta\rho$ and $\mathbf{n}$ subject to the pointwise constraint $\mathbf{n} \cdot \mathbf{n} = 1$. The first three terms in (1) with coefficients a, b and c are a Landau–de Gennes expansion of the free energy and set the preferred value of $\delta\rho$ in the uniform state, q is the wavenumber of the layering, B is a nematic-smectic coupling parameter, $\mathcal{D}^2$ denotes the Hessian operator and K is the elastic constant. The functional (1) can be derived from density-functional theory (based on a molecular statistical description), analogous to earlier work on smectics [55, 56].

Noticing the fact that (1) depends only on elements of the dyad $\mathbf{n}_i \mathbf{n}_j$, Ball & Bedford [57] proposed to modify (1) by replacing $\mathbf{n}_i \mathbf{n}_j$ by a uniaxial representation $(Q/s + I_3/3)_{ij}$ for three-dimensional problems, leading to

$$F(\delta\rho, Q) = \int_\Omega \left[\frac{a}{2} (\delta\rho)^2 + \frac{b}{3} (\delta\rho)^3 + \frac{c}{4} (\delta\rho)^4 \right.$$
$$\left. + B \left| \mathcal{D}^2 \delta\rho + \frac{q^2}{3s} (3Q + sI_3) \delta\rho \right|^2 + \frac{K}{2} |\nabla Q|^2 \right]. \quad (2)$$

Here, s is the scalar order parameter, I_d ($d \in \{2, 3\}$) is the identity matrix, and Q is a tensor-valued order parameter. They proved existence of minimizers of their modified model, but did not pursue any numerical analysis, or realize any implementation. One can anticipate numerical difficulties caused by having s on the denominator, as it is likely to be near zero for defect structures of physical interest.

Inspired by the modification from Ball & Bedford [57],

we propose the following alternative energy functional:

$$F(\delta\rho, Q) = \int_\Omega \left[\frac{a}{2} (\delta\rho)^2 + \frac{b}{3} (\delta\rho)^3 + \frac{c}{4} (\delta\rho)^4 \right.$$
$$+ B \left| \mathcal{D}^2 \delta\rho + q^2 \left(Q + \frac{I_d}{d} \right) \delta\rho \right|^2$$
$$\left. + \frac{K}{2} |\nabla Q|^2 + f_n(Q) \right], \quad (3)$$

where the nematic bulk energy density $f_n(Q)$ is $-l \left(\mathrm{tr}(Q^2) \right) + l \left(\mathrm{tr}(Q^2) \right)^2$ in two dimensions and $-\frac{l}{2} \left(\mathrm{tr}(Q^2) \right) - \frac{l}{3} \left(\mathrm{tr}(Q^3) \right) + \frac{l}{2} \left(\mathrm{tr}(Q^2) \right)^2$ in three dimensions.

We pause to contrast (3) with Ball & Bedford's formulation (2). In order to avoid possible numerical issues caused when $s \approx 0$, we instead weakly enforce $s = 1$ by adding the nematic bulk term f_n. The global minimizer of the nematic bulk energy $\int_\Omega f_n(Q)$ is known to be a uniaxial Q-tensor with scalar order parameter $s = 1$ [58, Proposition 15]. Thus, inclusion of this term both promotes the favorable scalar order parameter and a tendency towards a uniaxial expression for Q.

A substantial difficulty in obtaining the numerical solution of the minimization problem with (3) arises from the presence of the Hessian term, which requires $\delta\rho \in \mathcal{H}^2$ (i.e., square-integrable functions with square-integrable first and second derivatives). A *conforming* discretization requires the use of $\mathcal{C}^1$-continuous elements. Constructing these finite elements is quite involved in practice, especially in the three dimensional case. We therefore turn to the use of nonconforming discretizations following the so-called $\mathcal{C}^0$ *interior penalty* approach [59]. Essentially, we use $\mathcal{C}^0$-conforming elements and penalize inter-element jumps in the first derivatives to weakly enforce $\mathcal{C}^1$-conformity. To this end, we add a penalty term to the energy functional (3), leading to

$$F_\gamma(\delta\rho, Q) := F(\delta\rho, Q) + \sum_{e \in \mathcal{E}_I} \int_e \frac{\gamma}{2h_e^3} \left([\![\nabla \delta\rho]\!] \right)^2. \quad (4)$$

Here, γ is the penalty parameter (we fix $\gamma = 1$ throughout this work), $\mathcal{E}_I$ is the set of interior facets (edges/faces) of a mesh, h_e denotes the size of e, and the jump operator of a vector ∇w on a facet e of two adjacent cells, labelled K_- and K_+, is defined to be $[\![\nabla w]\!] = (\nabla w)_- \cdot \nu_- + (\nabla w)_+ \cdot \nu_+$ with ν_- and ν_+ denoting the restriction of the outward normal to K_- and K_+, respectively. The numerical analysis of this discretization will be reported elsewhere. Using $\mathcal{C}^0$ interior penalty methods has the advantages of both convenience and efficiency: the weak form is simple, with only minor modifications from a conforming method, and fewer degrees of freedom are used than with a fully discontinuous method.

III. NUMERICAL EXPERIMENTS

We now apply our discretization of (3) to a class of problems that encompasses commonly used techniques to induce self-organized structures in smectics. The liquid crystal is confined between two substrates treated to promote different preferred molecular orientations and must somehow interpolate between them, but unlike a nematic liquid crystal that can achieve this smoothly, a smectic may be prevented from doing so due to the layer constraint.

A. Solver details

Throughout this work, we use $\mathcal{C}^0$-continuous finite-element pairs for $(\delta\rho, Q)$ with the interior penalty term. In two dimensions, we use quadrilateral meshes where the space $\mathbb{CG}_k$ is given by tensor products of polynomials of up to degree k in each coordinate direction, yielding the spaces of piecewise biquadratic functions for $\mathbb{CG}_2$ and piecewise bicubic functions for $\mathbb{CG}_3$. We restrict Q to be a symmetric and traceless tensor, so it has two independent components in two dimensions. We thus seek the components of Q in $\mathbb{CG}_2^2$ and $\delta\rho$ in $\mathbb{CG}_3$. We use hexahedral meshes in three dimensions with similar tensor-product spaces, yielding the space of piecewise triquadratic functions for $\mathbb{CG}_2$ and piecewise tricubic functions for $\mathbb{CG}_3$. In three dimensions, Q has five independent components, so we seek its components in $\mathbb{CG}_2^5$, while retaining $\delta\rho$ in $\mathbb{CG}_3$.

Since the PDE problem to be solved is nonlinear, we use Newton's method with L^2 linesearch [60, Algorithm 2] as the outer nonlinear solver. The nonlinear solve is deemed to have converged when the Euclidean norm of the residual falls below 10^{-8}, or reduces from its initial value by a factor of 10^{-8}, whichever comes first. For the inner solves, the linearized systems are solved using the sparse LU factorization library MUMPS [61]. The solver described above is implemented in the Firedrake [62] library, which relies on PETSc [63] for solving the resulting linear systems. The mesh scale, h_e, employed in the $\mathcal{C}^0$ interior penalty approach is chosen to be the average of the diameters of the cells on either side of an edge.

Code availability—For reproducibility, both the solver code [64] and the exact version of Firedrake used [65] to produce the numerical results of this paper have been archived on Zenodo. An installation of Firedrake with components matching those used in this paper can be obtained by following the instructions at `https://www.firedrakeproject.org/download.html` with

`python3 firedrake-install --doi 10.5281/zenodo.4441123`

Defcon version #11e883c should then be installed, as described in `https://bitbucket.org/pefarrell/defcon/`.

B. Scenario I: defect free

As a simple example, proposed in the classic work of Williams & Kléman [54] to examine the bending effect in smectics, we consider a rectangle $\Omega = (-2, 2) \times (0, 2)$ with boundary labels

$$\Gamma_l = \{(x,y) : x = -2\}, \qquad \Gamma_r = \{(x,y) : x = 2\},$$
$$\Gamma_b = \{(x,y) : y = 0\}, \qquad \Gamma_t = \{(x,y) : y = 2\},$$

and impose the director $\mathbf{n}_e = (\cos\theta_0, -\sin\theta_0)$ for fixed $\theta_0 \in [0, \pi/2]$ at the lower boundary Γ_b and $\mathbf{n}_e = (\cos\theta_0, \sin\theta_0)$ at the upper boundary Γ_t. The corresponding boundary data for the Q-tensor derived from $\mathbf{n}_e$ is then given by

$$Q = \begin{bmatrix} (\cos\theta_0)^2 - \frac{1}{3} & -\cos\theta_0\sin\theta_0 & 0 \\ -\cos\theta_0\sin\theta_0 & (\sin\theta_0)^2 - \frac{1}{3} & 0 \\ 0 & 0 & -\frac{1}{3} \end{bmatrix} \quad \text{on } \Gamma_b,$$

$$Q = \begin{bmatrix} (\cos\theta_0)^2 - \frac{1}{3} & \cos\theta_0\sin\theta_0 & 0 \\ \cos\theta_0\sin\theta_0 & (\sin\theta_0)^2 - \frac{1}{3} & 0 \\ 0 & 0 & -\frac{1}{3} \end{bmatrix} \quad \text{on } \Gamma_t.$$

Furthermore, periodic boundary conditions for Q-tensor on the left and right boundaries, Γ_l and Γ_r are enforced. We discretize the domain Ω into 90×30 quadrilateral elements and specify the values of parameters in this experiment:

$$a = -10, \ b = 0, \ c = 10, \ B = 10^{-5}, \ K = 0.3,$$
$$q = 30, \ l = 30 \text{ and } w = 10.$$

Hence, the final form of the functional to be minimized in this scenario is

$$F_\gamma(\delta\rho, Q) = \int_\Omega \left(\frac{a}{2}(\delta\rho)^2 + \frac{b}{3}(\delta\rho)^3 + \frac{c}{4}(\delta\rho)^4 \right.$$
$$+ B\left| \mathcal{D}^2\delta\rho + q^2\left(Q + \frac{I_2}{2}\right)\delta\rho \right|^2$$
$$\left. + \frac{K}{2}|\nabla Q|^2 - l\left(\text{tr}\left(Q^2\right)\right) + l\left(\text{tr}\left(Q^2\right)\right)^2 \right)$$
$$+ \sum_{e \in \mathcal{E}_I} \int_e \frac{1}{2h_e^3}\left(\llbracket \nabla\delta\rho \rrbracket\right)^2. \tag{5}$$

For $\theta_0 = 0$, the boundary conditions become identical and the resulting configuration is with the layers extending vertically between the substrates in the "bookshelf" geometry. As θ_0 is increased from zero, the boundary conditions impose a bend deformation on the smectic. This can be accommodated in several ways: by distributing the deformation over the vertical direction (Fig. 1B); by localizing the bend to a region in the center with the layers flat and tilted in opposite directions in the top and bottom of the domain (Fig. 1C); or by introducing edge disclinations to relieve the cost of elastic deformation (Fig. 1D,E).
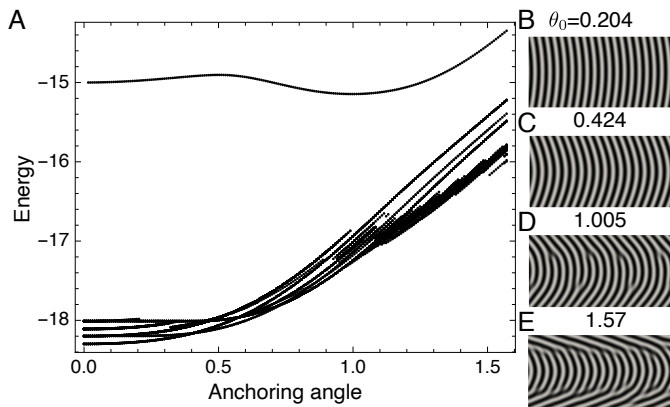
Figure 1. **Applying a bend deformation** to a smectic liquid crystal. **A** Bifurcation diagram. **B-E** Stationary solutions for different values of θ_0. The visualization displays the density perturbation $\delta\rho$.

The equilibrium structure as a function of θ_0 is hence determined by an energetic competition between the cost of bending and the cost of introducing disclinations. Using a technique called *deflation* [66], we can compute a bifurcation diagram for this scenario and quantitatively determine which of these solutions is the ground state as a function of θ_0 (Fig. 1A).

Further, we present more details about solutions found using the deflation technique in our implementation of the defect-free experiment. In Fig. 2, we show some computed stationary states as a function of θ_0. For each state, we display the value of the energy functional

$$
F(\delta\rho, Q) = \int_\Omega \left(\frac{a}{2} (\delta\rho)^2 + \frac{b}{3} (\delta\rho)^3 + \frac{c}{4} (\delta\rho)^4 \right.
$$
$$
+ B \left| \mathcal{D}^2 \delta\rho + q^2 \left(Q + \frac{I_2}{2} \right) \delta\rho \right|^2
$$
$$
\left. + \frac{K}{2} |\nabla Q|^2 - l \left(\mathrm{tr}\left(Q^2\right)\right) + l \left(\mathrm{tr}\left(Q^2\right)\right)^2 \right).
$$

For each column (i.e. fixed value of θ_0), we organize the stationary states in an energy-decreasing order. The bottom row depicts the lowest-energy states found. Readers may refer to [67] for an additional video illustrating the lowest energy solutions found as θ_0 is varied.

C. Scenario II: focal conic domains

A more extreme scenario is where the preferred alignment axes at each surface are perpendicular: one favors planar and the other vertical alignment. The experimentally observed configurations in this case are known as *toroidal focal conic domains* (TFCDs): the smectic layers adopt a configuration consisting of stacked interior sections of tori, with a central line defect extending between the two substrates. TFCDs may exist as isolated domains

in a background of vertically oriented smectic layers, or may self-assemble into a hexagonal lattice [37, 38, 44, 45]. If one of the boundary conditions is perturbed, such as by introducing a small preferred tilt at either substrate, asymmetric FCDs may arise where the layers form from sections of Dupin cyclides [37, 44].

To avoid a directional bias observed in numerical solutions with tetrahedra, we consider and discretize the cuboid $\Omega = (-1.5, 1.5) \times (-1.5, 1.5) \times (0, 2)$, with six labelled boundary faces

$$
\Gamma_{left} = \{(x, y, z) : x = -1.5\}, \quad \Gamma_{right} = \{(x, y, z) : x = 1.5\},
$$
$$
\Gamma_{back} = \{(x, y, z) : y = -1.5\}, \quad \Gamma_{front} = \{(x, y, z) : y = 1.5\},
$$
$$
\Gamma_{bottom} = \{(x, y, z) : z = 0\}, \quad \Gamma_{top} = \{(x, y, z) : z = 2\},
$$

into $6 \times 6 \times 5$ uniform hexahedra. Regarding boundary conditions, we use the following surface energy

$$
f_s(Q) = \int_{\Gamma_{bottom}} \frac{w}{2} |Q - Q_{radial}|^2 + \int_{\Gamma_{top}} \frac{w}{2} |Q - Q_{vertical}|^2,
$$
(6)

where w denotes the weak anchoring weight,

$$
Q_{radial} = \begin{bmatrix} \frac{x^2}{x^2+y^2} - \frac{1}{3} & \frac{xy}{x^2+y^2} & 0 \\ \frac{xy}{x^2+y^2} & \frac{y^2}{x^2+y^2} - \frac{1}{3} & 0 \\ 0 & 0 & -\frac{1}{3} \end{bmatrix}
$$

represents an in-plane (x-y plane) radial configuration of the director, and

$$
Q_{vertical} = \begin{bmatrix} -\frac{1}{3} & 0 & 0 \\ 0 & -\frac{1}{3} & 0 \\ 0 & 0 & \frac{2}{3} \end{bmatrix}
$$

gives a vertical (i.e., along the z-axis) alignment configuration of the director. For the FCD scenario, we only change the top boundary condition to perturb the preferred tilted director configuration. We perturb the angle between the director and the z-axis on the top surface Γ_{top} by θ_c, thus adopting

$$
Q_c = \begin{bmatrix} -\frac{1}{3} & 0 & 0 \\ 0 & (\sin(\theta_c))^2 - \frac{1}{3} & \sin(\theta_c)\cos(\theta_c) \\ 0 & \sin(\theta_c)\cos(\theta_c) & (\cos(\theta_c))^2 - \frac{1}{3} \end{bmatrix}
$$

instead of $Q_{vertical}$ in (6). Note that when taking $\theta_c = 0$, we return to the TFCD case.

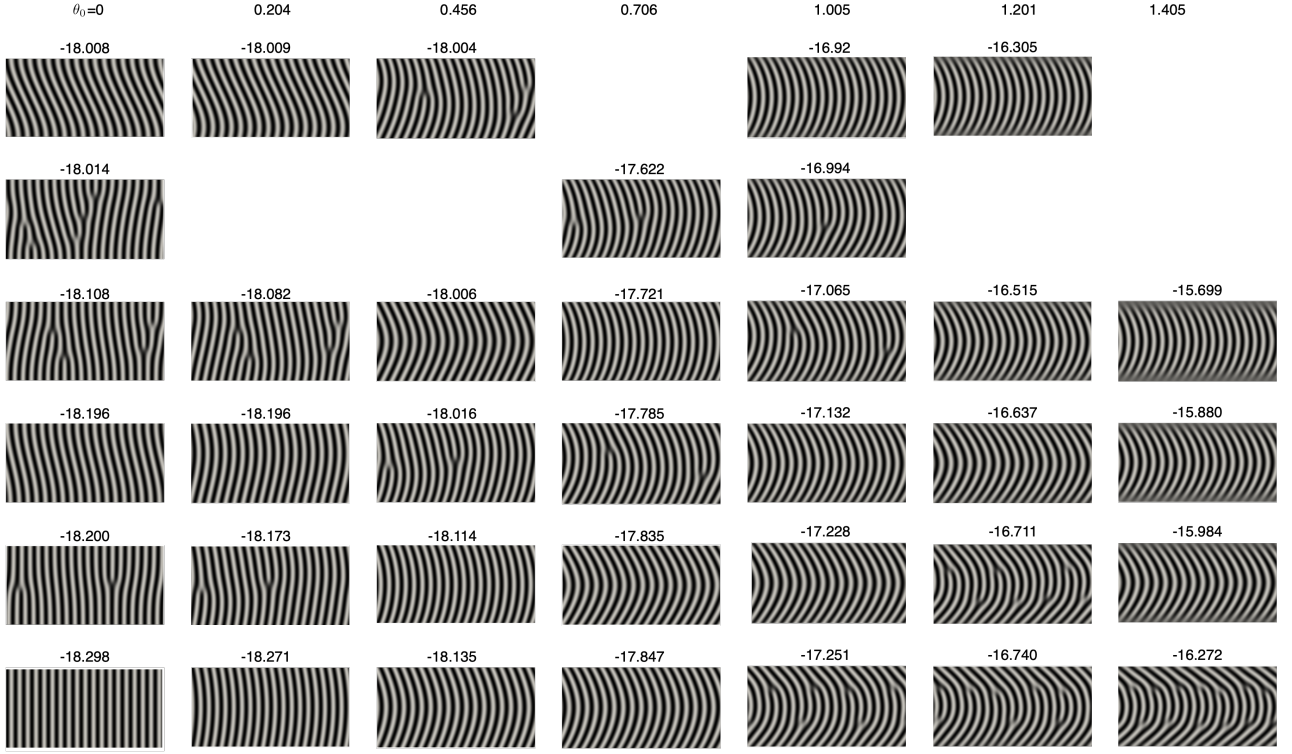Therefore, the final form of the functional to be mini-

$\theta_0=0$	0.204	0.456	0.706	1.005	1.201	1.405
-18.008	-18.009	-18.004			-16.92	-16.305
-18.014			-17.622	-16.994		
-18.108	-18.082	-18.006	-17.721	-17.065	-16.515	-15.699
-18.196	-18.196	-18.016	-17.785	-17.132	-16.637	-15.880
-18.200	-18.173	-18.114	-17.835	-17.228	-16.711	-15.984
-18.298	-18.271	-18.135	-17.847	-17.251	-16.740	-16.272

Figure 2. **Stationary states in the defect-free scenario.** Stationary states obtained at different values of θ_0. For each solution, the value of the energy functional is displayed above it. The bottom row depicts the lowest energy solution found for each value of θ_0.

mized in the FCD scenario is

$$
\begin{aligned}
F_\gamma(\delta\rho, Q) = \int_\Omega &\left(\frac{a}{2}\left(\delta\rho\right)^2 + \frac{b}{3}\left(\delta\rho\right)^3 + \frac{c}{4}\left(\delta\rho\right)^4 \right. \\
&+ B\left| \mathcal{D}^2\delta\rho + q^2\left(Q + \frac{I_3}{3}\right)\delta\rho \right|^2 \\
&+ \frac{K}{2}|\nabla Q|^2 \\
&\left. - \frac{l}{2}\left(\mathrm{tr}(Q^2)\right) - \frac{l}{3}\left(\mathrm{tr}(Q^3)\right) + \frac{l}{2}\left(\mathrm{tr}(Q^2)\right)^2 \right) \\
&+ \int_{\Gamma_{bottom}} \frac{w}{2}|Q - Q_{radial}|^2 + \int_{\Gamma_{top}} \frac{w}{2}|Q - Q_c|^2 \quad (7) \\
&+ \sum_{e \in \mathcal{E}_I} \int_e \frac{1}{2h_e^3}\left(\llbracket \nabla\delta\rho \rrbracket\right)^2.
\end{aligned}
$$

Since Newton's method is employed as the nonlinear solver, we take the following initial guesses:

$$
\delta\rho = \cos(6\pi z), \quad Q = Q_{ic},
$$

where $Q_{ic} = \left(\mathbf{n}_{ic} \otimes \mathbf{n}_{ic} - \frac{I_3}{3}\right)$ with

$$
\mathbf{n}_{ic} = \frac{1}{m}\begin{bmatrix} x\left(\sqrt{x^2+y^2} - R\right) \\ y\left(\sqrt{x^2+y^2} - R\right) \\ z\left(\sqrt{x^2+y^2}\right) \end{bmatrix},
$$

and

$$
m = \sqrt{x^2+y^2}\sqrt{\left(R - \sqrt{x^2+y^2}\right)^2 + z^2}.
$$

Here, the initial guess for the Q-tensor is computed from the mathematical representation for a family of tori, and we have taken a major radius $R = 1.5$ in our implementation. The values of parameters used in the (T)FCD experiments are also specified:

$$
a = -10, \ b = 0, \ c = 10, \ B = 10^{-3}, \ K = 0.03,
$$
$$
q = 10, \ l = 30 \text{ and } w = 10.
$$

Despite the centrality of TFCDs in the study of smectics, and for applications, prior numerical work on them has been limited to finding solutions using modifications of the nematic theory [43]. We therefore verify that FCDs are stationary solutions of our functional (3) and characterize their response to tilted boundary conditions Q_c by perturbing the zenith angle θ_c between the director and the z-axis in the boundary configuration.

Displayed in Fig. 3 is a sequence of solutions as a function of θ_c, the preferred tilt away from the vertical at the upper substrate. As can be seen in Fig. 3C, we recover the cylindrically symmetric TFCD for $\theta_c = 0$; as $\theta_c > 0$ the solution becomes asymmetric (Fig. 3C) and the central defect line becomes a hyperbola, as expected from geometry [3, 4, 18].
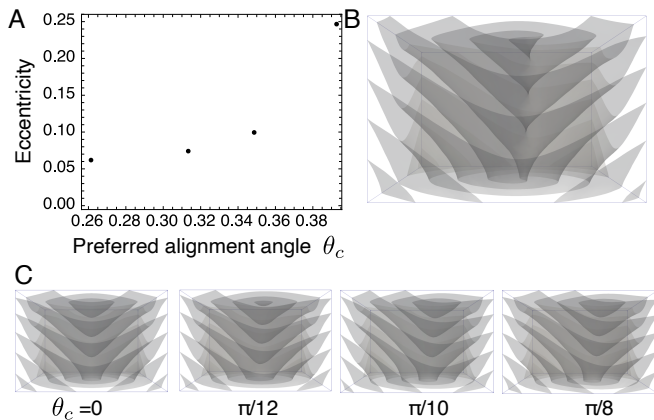
Figure 3. Focal conic domains under tilted boundary conditions. **A** Eccentricity of solution as a function of preferred tilt angle θ_c. **B** Solution with single screw dislocation defect. **C** Stationary solutions for different values of θ_c. Images **B** and **C** display zero isosurfaces of the density variation $\delta\rho$, to visualize the layer structure of the smectic.

We further observe some interesting structures found in this simulation, e.g., single screw dislocation defect as shown in Fig. 3B. To illustrate the internal structure of the layers for the solution patterns, we refer to three videos (see [67]), presenting FCD, single and double screw dislocations for $\theta_c = \pi/12$. They depict the zero-isosurfaces of the smectic density variation field $\delta\rho$ and the isosurfaces are colored by height (the z-coordinate) to assist in depth perception.

D. Scenario III: oily streaks

For sufficiently thin films, the elastic energy cost of two dimensional curvature of the layers observed in the FCD solutions becomes prohibitive. Instead, the smectic adopts a configuration referred to as an "oily streak" texture [21, 41, 43]. The structure is periodic in one direction parallel to the substrate and spatially uniform in the other tangential direction; the periodicity L is experimentally found to increase linearly with the film thickness τ such that $L \approx L_0 + 4.5\tau$ [42]. Addition of chiral dopants can be used to control the orientation of the streaks [41].

X-ray diffraction experiments for films $0.15\mu m \leq \tau \leq 0.35\mu m$ $(47 - 110$ layers) indicate that the smectic layer normals are continuously and uniformly distributed in orientation with a significant additional peak for smectic layers that are parallel to the plane of the substrate. An approximate layer structure proposed by Michel et al. [42] consistent with this data comprises periodic units incorporating sections of cylinders joined to planes oriented parallel to the substrate (Fig. 4A). This structure implies, however, significant deformations of the free interface with singular points between units; while undulations of the smectic-air interface are observed by atomic force microscopy, the amplitude is only around $1/5$ of the film thickness once the finite size of the tip is accounted for. To address this, the same authors consider more complex structures incorporating curvature walls [21, 43] (Fig. 4B) that necessarily imply local dilation of the layers or local melting into the nematic phase along walls between units.

For even thinner films $\tau \sim 70nm$ (approx. 22 layers), X-ray diffraction reveals an apparent excess of the planar region that cannot be explained by either structure discussed so far [43]; a possible structure that does so, and is consistent with the X-ray data, is depicted in Fig. 4C and incorporates an approximately hemicylindrical Rotating Grain Boundary (RGB) that partitions the cylindrical component from the planar component. Such a structure, with abruptly discontinuous layers, is energetically very costly and was envisioned in [43] as a mesoscopic approximation: at the nanoscopic level, the RGB might contain a network of dislocations to include the additional layers, or locally melt into the nematic phase along the RGB.

Hence, while these *ansatz* models are very helpful in that they provide an overall understanding of the structure and facilitate interpretation of the experimental data, they incorporate coarse-grained features such as the RGBs and, moreover, they are not calculated stationary states of an appropriate free energy functional. Understanding the detailed structure of the oily streaks therefore remains an important open problem.

Let r denote the aspect ratio of a rectangle $\Omega = (-r, r) \times (0, 2)$. To simulate oily streaks in the rectangle, Ω, we weakly impose a planar (i.e., horizontal) boundary condition on the bottom face and a homeotropic (i.e., vertical) condition on the top surface. We label the different boundaries of the rectangle as

$$\Gamma_l = \{(x, y) : x = -r\}, \qquad \Gamma_r = \{(x, y) : x = r\},$$
$$\Gamma_b = \{(x, y) : y = 0\}, \qquad \Gamma_t = \{(x, y) : y = 2\}.$$

Then the following surface energy is imposed:

$$f_s(Q) = \int_{\Gamma_b} \frac{w}{2} |Q - Q_{bottom}|^2 + \int_{\Gamma_t \cup \Gamma_l \cup \Gamma_r} \frac{w}{2} |Q - Q_{top}|^2,$$

where w is the weak anchoring weight and two weakly prescribed configurations Q_{bottom} and Q_{top} are given by

$$Q_{bottom} = \begin{bmatrix} \frac{1}{2} & 0 \\ 0 & -\frac{1}{2} \end{bmatrix},$$

yielding horizontally aligned directors, and

$$Q_{top} = \begin{bmatrix} -\frac{1}{2} & 0 \\ 0 & \frac{1}{2} \end{bmatrix},$$

yielding vertically aligned directors.

In this aspect-ratio continuation experiment, we always discretize the domain Ω into 90×30 quadrilateral elements, even as we change the domain size by varying
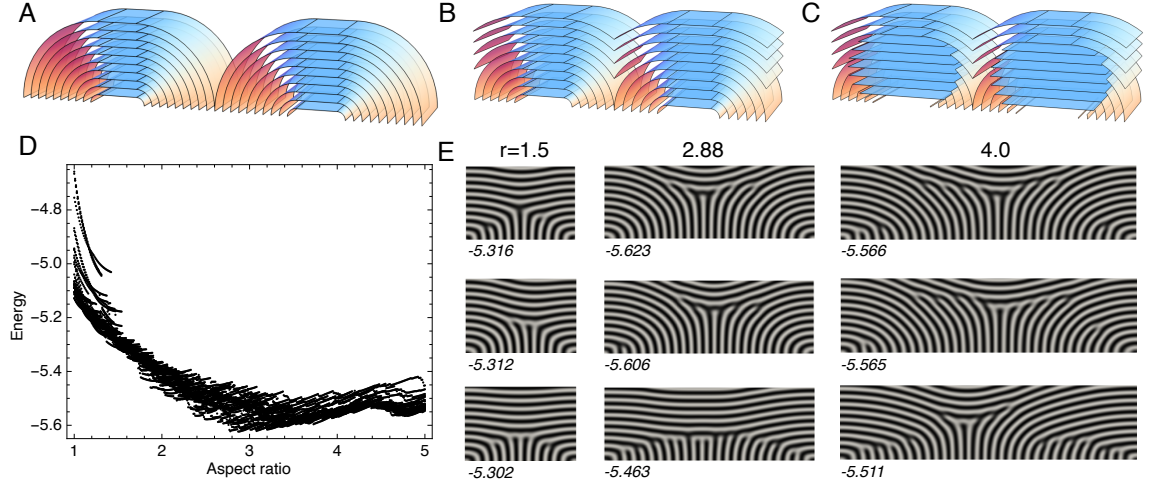
Figure 4. **Oily streaks. A-C** Candidate structures proposed in Michel et al. [42] consistent with X-ray diffraction. **D** Bifurcation diagram of structures as a function of aspect ratio. **E** Selected stationary states obtained at different aspect ratio r. The top row represents the lowest energy solution found.

the aspect ratio, r. Hence, the final form of the functional to be minimized in this scenario is

$$F_\gamma(\delta\rho, Q) = \int_\Omega \left(\frac{a}{2} \left(\delta\rho\right)^2 + \frac{b}{3} \left(\delta\rho\right)^3 + \frac{c}{4} \left(\delta\rho\right)^4 \right.$$

$$+ B \left| \mathcal{D}^2\delta\rho + q^2 \left(Q + \frac{I_2}{2} \right) \delta\rho \right|^2$$

$$\left. + \frac{K}{2} |\nabla Q|^2 - l \left(\operatorname{tr}\left(Q^2\right) \right) + l \left(\operatorname{tr}\left(Q^2\right) \right)^2 \right)$$

$$+ \int_{\Gamma_b} \frac{w}{2} |Q - Q_{bottom}|^2 \tag{8}$$

$$+ \int_{\Gamma_t \cup \Gamma_l \cup \Gamma_r} \frac{w}{2} |Q - Q_{top}|^2$$

$$+ \sum_{e \in \mathcal{E}_I} \int_e \frac{1}{2h_e^3} \left([\![\nabla\delta\rho]\!] \right)^2. \tag{9}$$

We take the following initial guesses for $\delta\rho$ and Q:

$$\delta\rho = 1, \quad Q = Q_{os},$$

where $Q_{os} = (\mathbf{n}_{os} \otimes \mathbf{n}_{os} - \frac{I_2}{2})$ with

$$\mathbf{n}_{os} = \frac{1}{m} \begin{bmatrix} x \left(|x| - R\right) \\ (|x|) \, y \end{bmatrix},$$

and

$$m = |x| \sqrt{\left(R - |x|\right)^2 + y^2}.$$

Here, the initial guess for the Q-tensor is computed from a simplified two-dimensional mathematical representation of a family of tori, and we have taken the major radius $R = 1$. Finally, we specify the values of parameters used in this experiment:

$$a = -10, \ b = 0, \ c = 10, \ B = 10^{-5}, \ K = 0.3,$$

$$q = 30, \ l = 1 \text{ and } w = 10.$$

We again use the deflation technique to explore the stationary states of (9) on the rectangular domain Ω of fixed vertical dimension and varying aspect ratio r. For simplicity we do not allow for variation of the free surface, which will be an area of future work, but instead impose weak anchoring conditions. Furthermore, a video showing the lowest energy configurations as the aspect ratio r varies is included in [67].

A partially enumerated energy landscape is displayed in Fig. 4D, showing an extremely dense thicket of solutions, but qualitatively supporting earlier work in that an overall minimizer occurs at an aspect ratio of around 3, which is similar to experimental values even with no parameter tuning performed here. Close examination of the energy landscape, together with the corresponding solution set, shows many small discontinuous jumps that result from delicate commensurability effects, whereby certain sizes of domain are compatible with a given periodicity of the layers as well as from variations in the number of defects and their detailed placement. Similar effects have been observed when other periodic liquid crystals such as cholesterics are confined in domains that promote geometric frustration [68].

The solution set obtained contains examples reminiscent of previously proposed structures (Fig. 4E). The minimum energy states found at different aspect ratio contain cylindrical sections mediated by a defect-filled region reminiscent of the mesoscopic rotating grain boundaries. Other solutions displayed in the lowest row of Fig. 4E are quite different from those heretofore proposed, where regions of relatively vertically oriented layers sit atop cylindrical regions interspersed with defects. Each of these incorporates a greater proportion of vertical layers relative to the hemicylindrical-planar *ansatz* of Fig. 4A,B and may provide alternative structures for oily

streaks in ultrathin films. In future work, the boundary conditions at the top interface should be carefully reconsidered, including the incorporation of a free interface.

IV. CONCLUSION

We have formulated a free energy functional for smectics that is amenable to finite element simulation, and applied it to scenarios involving boundary conditions that are incompatible with uniform smectic order; our new model successfully reproduces, even without careful tuning of parameters, a number of experimentally observed and theoretically expected phenomena, as well as producing new candidate structures for thin smectic films that are explicitly stationary states of an energy functional. We also demonstrate how to overcome a less obvious difficulty with numerical studies of smectics and layered media generally: the solution landscapes are extremely dense due to the presence of defects. The combination of our model together with the deflation technique enables detailed exploration of this landscape, enabling us to isolate both the ground state and low-lying excited states that may be observed in physical systems.

---

[1] P. G. de Gennes, Solid State Commun. **10**, 753 (1972).
[2] C. S. Rosenblatt, R. Pindak, N. A. Clark, and R. B. Meyer, Journal de Physique **38**, 1105 (1977).
[3] M. Kléman and O. D. Lavrentovich, Physical Review E **61**, 1574 (2000).
[4] M. Kléman and O. D. Lavrentovich, Liquid Crystals **36**, 1085 (2009).
[5] I. W. Stewart, Liquid Crystals **15**, 859 (1993).
[6] G. Friedel and F. Grandjean, Bulletin de la Société Française de Minéralogie **33**, 409 (1910).
[7] J. P. Bramble, S. D. Evans, J. R. Henderson, T. J. Atherton, and N. J. Smith, Liquid Crystals **34**, 1137 (2007).
[8] W. Guo, S. Herminghaus, and C. Bahr, Langmuir **24**, 8174 (2008).
[9] E. Smela and L. J. Martinez-Miranda, Journal of Applied Physics **73**, 3299 (1993).
[10] M. C. Choi, T. Pfohl, Z. Wen, Y. Li, M. W. Kim, J. N. Israelachvili, and C. R. Safinya, Proceedings of the National Academy of Sciences of the United States of America **101**, 17340 (2004).
[11] T. Ohzono, Y. Takenaka, and J.-i. Fukuda, Soft Matter **8**, 6438 (2012).
[12] R. S. Preusse, E. R. George, S. A. Aghvami, T. M. Otchy, and M. A. Gharbi, Soft Matter **16**, 8352 (2020).
[13] A. Honglawan, D. A. Beller, M. Cavallaro, R. D. Kamien, K. J. Stebe, and S. Yang, Proceedings of the National Academy of Sciences **110**, 34 (2013).
[14] Y. Xia, A. A. DeBenedictis, D. S. Kim, S. Chen, S.-U. Kim, D. J. Cleaver, T. J. Atherton, and S. Yang, Nature Communications **10**, 5104 (2019).
[15] T. Lopez-Leon and A. Fernandez-Nieves, Colloid and Polymer Science **289**, 345 (2011).
[16] M. Urbanski, C. G. Reyes, J. Noh, A. Sharma, Y. Geng, V. S. R. Jampani, and J. P. F. Lagerwall, Journal of Physics: Condensed Matter **29**, 133003 (2017).
[17] X. Xing, H. Shin, M. J. Bowick, Z. Yao, L. Jia, and M.-H. Li, Proceedings of the National Academy of Sciences **109**, 5202 (2012), 1108.4763.
[18] C. Blanc and M. Kléman, The European Physical Journal E **4**, 241 (2001).
[19] M. A. Gharbi, I. B. Liu, Y. Luo, F. Serra, N. D. Bade, H.-N. Kim, Y. Xia, R. D. Kamien, S. Yang, and K. J. Stebe, Langmuir **31**, 11135 (2015).
[20] F. Serra, M. A. Gharbi, Y. Luo, I. B. Liu, N. D. Bade, R. D. Kamien, S. Yang, and K. J. Stebe, Advanced Optical Materials **3**, 1287 (2015), 1505.01449.
[21] J.-P. Michel, E. Lacaze, M. Alba, M. de Boissieu, M. Gailhanou, and M. Goldmann, Physical Review E **70**, 011709 (2004).
[22] Y. H. Kim, D. K. Yoon, H. S. Jeong, O. D. Lavrentovich, and H. Jung, Advanced Functional Materials **21**, 610 (2011).
[23] D. P. Singh, R. Visvanathan, A. E. Duncan, B. Duponchel, Y. Boussoualem, S. Kumar, N. A. Clark, J.-F. Blach, R. Douali, and A. Daoudi, Liquid Crystals **46**, 1 (2018).
[24] I. Gryn, E. Lacaze, L. Carbone, M. Giocondo, and B. Zappone, Advanced Functional Materials **26**, 7122 (2016).
[25] S.-P. Do, A. Missaoui, A. Coati, D. Coursault, H. Jeridi, A. Resta, N. Goubet, M. M. Wojcik, A. Choux, S. Royer, E. Briand, B. Donnio, J. L. Gallani, B. Pansu, E. Lhuillier, Y. Garreau, D. Babonneau, M. Goldmann, D. Constantin, B. Gallas, B. Croset, and E. Lacaze, Nano Letters **20**, 1598 (2020).
[26] A. Honglawan, D. S. Kim, D. A. Beller, D. K. Yoon, M. A. Gharbi, K. J. Stebe, R. D. Kamien, and S. Yang, Soft Matter **11**, 7367 (2015).
[27] Y. Mai and A. Eisenberg, Chemical Society Reviews **41**, 5969 (2012).
[28] H. Hu, M. Gopinadhan, and C. O. Osuji, Soft Matter **10**, 3867 (2014).
[29] M. Selmi, J.-C. Loudet, P. V. Dolganov, T. Othman, and P. Cluzeau, Soft Matter **13**, 3649 (2017).
[30] L. S. Hirst, A. Ossowski, M. Fraser, J. Geng, J. V. Selinger, and R. L. B. Selinger, Proceedings of the National Academy of Sciences **110**, 3242 (2013).
[31] M. A. Gharbi, D. A. Beller, N. Sharifi-Mood, R. Gupta, R. D. Kamien, S. Yang, and K. J. Stebe, Langmuir **34**, 2006 (2018), 1709.08253.
[32] G. P. Alexander, B. G.-g. Chen, E. A. Matsumoto, and R. D. Kamien, Physical Review Letters **104**, 257802 (2010), 1004.0465.
[33] D. A. Beller, M. A. Gharbi, A. Honglawan, K. J. Stebe, S. Yang, and R. D. Kamien, Physical Review X **3**, 041026 (2013), 1310.6797.

[34] J. P. Sethna and M. Kléman, Physical Review A **26**, 3037 (1982).

[35] M. Kléman, Journal de Physique **38**, 1511 (1977).

[36] D. B. Liarte, M. Bierbaum, M. Zhang, B. D. Leahy, I. Cohen, and J. P. Sethna, Physical Review E **92**, 062511 (2015).

[37] M.-J. Gim, D. A. Beller, and D. K. Yoon, Nature Communications **8**, 15453 (2017).

[38] T. J. Atherton, R. Wang, and C. Rosenblatt, Physical Review E **77**, 061702 (2008).

[39] D. Coursault, J. Grand, B. Zappone, H. Ayeb, G. Lévi, N. Félidj, and E. Lacaze, Advanced Materials **24**, 1461 (2012).

[40] D. Coursault, B. Zappone, A. Coati, A. Boulaoued, L. Pelliser, D. Limagne, N. Boudet, B. H. Ibrahim, A. d. Martino, M. Alba, M. Goldmann, Y. Garreau, B. Gallas, and E. Lacaze, Soft Matter **12**, 678 (2015).

[41] I. R. Nemitz, A. J. Ferris, E. Lacaze, and C. Rosenblatt, Soft Matter **12**, 6662 (2016).

[42] E. Lacaze, J.-P. Michel, M. Alba, and M. Goldmann, Physical Review E **76**, 041702 (2007).

[43] J.-P. Michel, E. Lacaze, and M. Goldmann, Physical Review Letters **96**, 027803 (2006).

[44] B. Zappone, C. Meyer, L. Bruno, and E. Lacaze, Soft Matter **8**, 4318 (2012).

[45] P. E. Cladis and S. Torza, Journal of Applied Physics **46**, 584 (1975).

[46] B. Zappone, A. E. Mamuk, I. Gryn, V. Arima, A. Zizzari, R. Bartolino, E. Lacaze, and R. Petschek, Proceedings of the National Academy of Sciences **117**, 17643 (2020).

[47] L. J. Martinez-Miranda, Y. Shi, and S. Kumar, Molecular Crystals and Liquid Crystals Science and Technology. Section A. Molecular Crystals and Liquid Crystals **326**, 41 (1999).

[48] K. May, K. Harth, T. Trittel, and R. Stannarius, ChemPhysChem **15**, 1508 (2014).

[49] K. May, K. Harth, T. Trittel, and R. Stannarius, Europhysics Letters **100**, 16003 (2012).

[50] K. Harth, T. Trittel, K. May, and R. Stannarius, Soft Matter **15**, 6769 (2019), 1809.08082.

[51] M. Y. Pevnyi, J. V. Selinger, and T. J. Sluckin, Physical Review E **90**, 032507 (2014).

[52] J. M. Ball, Molecular Crystals and Liquid Crystals **647**, 1 (2017).

[53] J. P. Borthagaray, R. H. Nochetto, and S. W. Walker, Numerische Mathematik **145**, 837 (2020).

[54] C. E. Williams and M. Kléman, Le Journal de Physique Colloques **36**, C1 (1975).

[55] A. Linhananta and D. E. Sullivan, Physical Review A **44**, 8189 (1991).

[56] A. Poniewierski and T. J. Sluckin, Physical Review A **43**, 6837 (1991).

[57] J. M. Ball and S. J. Bedford, Molecular Crystals and Liquid Crystals **612**, 1 (2015).

[58] A. Majumdar and A. Zarnescu, Archive for Rational Mechanics and Analysis **196**, 227 (2010).

[59] S. C. Brenner, C^0 interior penalty methods, in *Frontiers in Numerical Analysis - Durham 2010. Lecture Notes in Computational Science and Engineering*, Vol. 85, edited by J. Blowey and M. Jensen (Springer, Berlin, Heidelberg, 2011).

[60] P. R. Brune, M. G. Knepley, B. F. Smith, and X. Tu, SIAM Review **57**, 535 (2015).

[61] P. R. Amestoy, I. Duff, and J.-Y. L'Excellent, Computer Methods in Applied Mechanics and Engineering **184**, 501 (2000).

[62] F. Rathgeber, D. A. Ham, L. Mitchell, M. Lange, F. Luporini, A. T. T. McRae, G. T. Bercea, G. R. Markall, and P. H. J. Kelly, ACM Transactions on Mathematical Software **43**, 1 (2017).

[63] S. Balay, S. Abhyankar, M. F. Adams, J. Brown, P. Brune, K. Buschelman, L. Dalcin, V. Eijkhout, W. D. Gropp, D. Kaushik, M. Knepley, L. C. McInnes, K. Rupp, B. F. Smith, and H. Zhang, *PETSc users manual*, Tech. Rep. ANL-95/11 - Revision 3.9 (Argonne National Laboratory, 2018).

[64] J. Xia, Smectic-A numerics (2021), 10.5281/zenodo.4432172.

[65] Zenodo/Firedrake-20210112.0, Software used in 'Structural Transitions in Geometrically Frustrated Smectics' (2021), 10.5281/zenodo.4441123.

[66] P. E. Farrell, Á. Birkisson, and S. Funke, SIAM Journal on Scientific Computing **37**, A2026 (2015).

[67] J. Xia, Structural transitions in geometrically frustrated smectics (supplementary materials) (2021), https://www.youtube.com/playlist?list=PLr8tas_dt-wwd81QWCyNZe51L7NckSfwo.

[68] D. B. Emerson, J. H. Adler, P. E. Farrell, S. P. MacLachlan, and T. J. Atherton, Liquid Crystals **45**, 341 (2017).